ADVANCED ENGINEERING MATERIALS
www.aem-journal.com

Intelligent Sensing System Based on Hybrid Nanogenerator by Harvesting Multiple Clean Energy

Yuhang Xie, Hulin Zhang, Guang Yao, Saeed Ahmed Khan, Min Gao, Yuanjie Su, Weiqing Yang, and Yuan Lin**

The inexhaustible mechanical kinetic energy can be extracted from wind and flowing water. Besides, flowing water also possesses electrostatic energy owing to the triboelectric charges caused by contacting with surrounding media, such as air. Here, a rotating hybridized triboelectric nanogenerator (TENG) has been established, by comprising of a water-TENG (W-TENG), a disk-TENG (D-TENG), and an electromagnetic generator (EMG), which has been explored for simultaneously harvesting energies from flowing water and wind. The W-TENG is fabricated by wheel blades, polyvinylidene fluoride (PVDF), superhydrophobic polytetrafluoroethylene (PTFE), and aluminum to harvest the electrostatic energy. Moreover, the flowing water and wind impact on the wheel blades also causes the rotation motion of D-TENG and EMG, resulting in being converted into electricity. At the rotation speed of 200 rpm, the short circuit current of D-TENG and EMG can reach 0.4 μA and 7 mA, respectively. The open circuit voltage of W-TENG can be up to 10 V at a flowing water rate of 60 ml s^{-1}. Besides, the hybridized NG is demonstrated to harvest water and wind energy and to act as a power source to charge a lithium battery or capacitor, which can drive LEDs, PH monitoring system, and wireless temperature and humidity sensing system. All these results show the potentials of the hybridized NG for harvesting multiple types of energies from the environment and constructing different self-powered systems.

Because of the rapid energy consumption and shortage in fossil fuel, energy crisis is becoming more and more serious than ever before. For the sustainable development of modern society, harvesting different kinds of energies from ambient environment has attracted increasing attention.[1–8] Recently, the hybridized TENG has been explored as a new technology to harvest various energies, such as vibration,[9,10] air flow,[11,12] water waves,[13,14] and rotation,[15,16] which is mainly based on contact electrification effect and electrostatic induction.[17–19]

Previously, most people used two solid materials contacting periodically to generate triboelectric charges on their interface.[20–25] Recently, triboelectric charges that are created between the interfaces of water and air are used to develop TENG widely.[26,27] The TENGs have been demonstrated a promising approach for scavenging energy from surrounding flowing medium. On the other hand, the flowing water and air has not only mechanical energy, but also electrostatic energy, which comes from the triboelectric charges in water generated during the process of contacting with pipe or air.[28] In previous reports, the researchers usually use a single energy harvesting device to grab a certain energy from flowing water and air.[29,30] However, in our demonstrations, to harvest multiple energies simultaneously, we have integrated D-TENG, W-TENG, and EMG into a hybrid energy harvester. In the W-TENG, we used PVDF and PTFE with nanostructures to enhance the forward output, which is better than by just using PTFE.[31] When the flowing water impacted on the wheel blades, the W-TENG begins to work and the mechanical energy from the water causes the rotation motion of D-TENG and EMG. The open circuit voltages of D-TENG, W-TENG, and EMG can get 500, 11, and 0.4 V, respectively. It is also demonstrated that, when the hybrid NG harvest energy from external environment, it can be used to construct different self-powered systems such as: display system, PH monitoring system, and wireless temperature and humidity sensing system. Comparing with traditional detecting systems powered by batteries, our self-powered sensor systems are independent of using batteries, which can save energy and improve the sustainability of sensing systems.

Dr. H. Zhang, Prof. Y. Lin, Dr. Y. Xie, Dr. G. Yao, Dr. S. A. Khan, Dr. M. Gao, Dr. Y. Su
State Key Laboratory of Electronic Thin Films and Integrated Devices
University of Electronic Science and Technology of China, Chengdu, 610054, China
E-mail: zhangd198710@gmail.com; linyuan@uestc.edu.cn

Dr. H. Zhang
Micro Nano System Research Center, Key Lab of Advanced Transducers and Intelligent Control System of the Ministry of Education & College of Information Engineering
Taiyuan University of Technology, Taiyuan 030024, China

Prof. W. Yang
Key Laboratory of Advanced Technologies of Materials (Ministry of Education), School of Materials Science and Engineering
Southwest Jiaotong University, Chengdu, 610031, China

The ORCID identification number(s) for the author(s) of this article can be found under https://doi.org/10.1002/adem.201700886.

DOI: 10.1002/adem.201700886

1. Experimental Section

1.1. Assembling of the D-TENG and W-TENG

In this work, the D-TENG has two parts: a stator and a rotator. For the rotator and the stator, acrylic sheet with thickness of

4 mm was shaped by a laser cutter to form disk substrate with diameter of 150 mm. Four fan-shaped Al electrodes with central angle of 30° were attached on the stator, which was fixed on the iron rod axis, and four copper conductors were drawn from the Al electrodes. For the rotator, four fan-shaped PTFE films with thickness of 50 μm and central angle of 30° were attached on the rotator, as is illustrated in **Figure 1**a. For the W-TENG, four wheel blades with 50 mm in length, 20 mm in width, and 4 mm in thickness were made by laser cutter. Every W-TENG is composed of Al electrode, polarized PVDF film, and PTFE film, which can harvest the electrostatic energy from flowing water. These three films with 50 μm in thickness were coated on the blades in sequence.

1.2. The Fabrication of the EMG

The EMG is also composed of two parts: a stator and a rotator. The stator with diameter of 150 mm and thickness of 4 mm was made by laser cutter. Four grooves with 2 mm in depth and 30 mm in diameter were cut on one side of the stator and four copper coils were embedded in the four grooves. Then, the stator was fixed on the iron rod axis and four copper coils were connected the together by copper conductors. For the rotator of the EMG, four grooves with 2 mm in depth and 30 mm in diameter were made by the same method on one side and four magnets with 30 mm in diameter were embedded in them.

2. Results and discussion

The structure of the hybridized NG is schematically illustrated in Figure 1a, which mainly consists of three parts: the D-TENG, the W-TENG, and the EMG. The real photograph of D-TENG is illustrated in Figure 1b consist of two parts: one is left disk with PTFE and the other is right disk with Al electrode. A smooth iron rod has been introduced which serves as the rotation axis of hybridized NG. The axis penetrates through the D-TENG. The right disk is fixed on the axis and keeps motionless. The left disk is connected with the axis by a bearing, which can reduce friction between the axis and the left disk. When the water or wind impacts on the wheel blades, the left disk can rotate freely. The W-TENG is composed of 4 wheel blades. Every blade is a single-electrode-based TENG to harvest the electrostatic energy from flowing water, in which the electrical channel is formed between the Al electrode on the blades and the ground. The real photograph of EMG is shown in Figure 1c, which consists of two components: one is coil-disk that contains 4 coils and the other is magnet-disk, that is, composed of 4 magnets. The coil-disk is fixed on the axis just like the right disk of D-TENG. The magnet-disk is similar to the left disk of D-TENG, which is also connected with the axis using a bearing.

For fabricating the water blades of W-TENG, a thin Al film with surface grown AAO nanopores was attached on a quadrate PET sheet to serve as the electrode. Then, a PVDF thin film that is covered by a PTFE layer with nanostructure was adhered on the Al film to operate as triboelectric material. The SEM image of Al film with nanostructure can be seen in the inset of Figure 1a. To transfer charges from W-TENG to peripheral equipment, the Al electrode was connected with the iron rod by copper wires. To fabricate the left disk of the D-TENG, a PTFE film was attached on an acrylic substrate and the right disk was made by Al film with nanostructure covering an acrylic substrate with four segments. The PTFE layer of the left disk and the Al layer of the right disk were brought to a face-to-face intimate contact to form a TENG operating in rotation mode.

The working mechanism of the D-TENG is based on the combination of triboelectric electrification and electrostatic

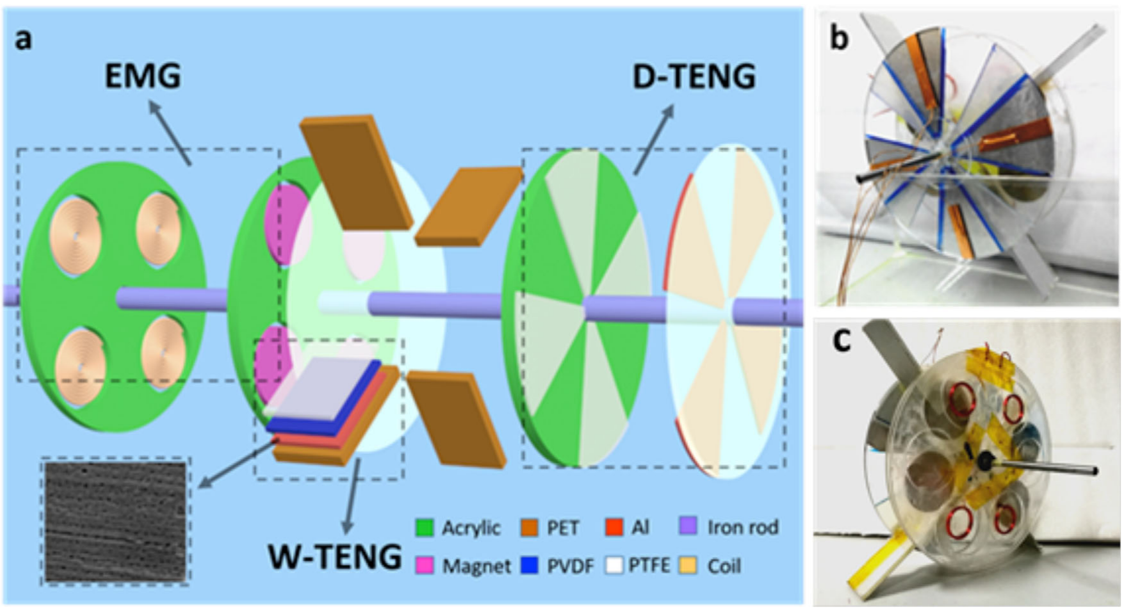

Figure 1. The structure diagram of the hybridized TENG. a) A 3D schematic illustrations of the functional components of hybridized NG and the inset is the SEM image of Al electrode (scale bar, 500 nm). b) The real photograph of D-TENG. c) The real photograph of EMG.

induction, which can be explained in four consecutive steps in a full rotation cycle, as illustrated in **Figure 2**. The corresponding numerical calculations of the potential distribution cross the D-TENG are also shown accordingly. In the first step, as illustrated in Figure 2a, before the left-disk acting as rotator starts to spin, no triboelectric charges were generated owing to lack of indispensable contact between PTFE and Al. In the second step, when the rotator starts to rotate, the PTFE thin film begins to contact with Al electrode and an equal amount of negative and positive charges will be generated on the PTFE layer and the Al foil, respectively, due to the difference in electron affinity between them, resulting in electrons on the Al foil being driven to the ground, as displayed in Figure 2b. In the third step, the PTFE film and the Al electrode are fully overlapped to establish an electric equilibrium, as shown in Figure 2c, thus, there is no electron transferred and, consequently, no current is generated. In the last step, the left disk continues to rotate and the contact area between PTFE film and Al electrode will decrease. The quantity of positive charges on Al electrode will reduce, which depicts that the electrons will transfer back to Al electrode from the ground and the disk of the two triboelectric layers will returns to its original position as shown in Figure 2d. As the left disk rotates continuously, the electricity generation will continue. Actually, the flowing water was used to drive the hybridized NG. The flowing water from the faucet has positive tribo-charges due to the contact electrification between the water and the pipe/air during its traveling. As the positively charged flowing water contacts and separates from the blade of W-TENG periodically, the electrons will transfer between Al electrode and the ground due to the electrostatic induction. Under the sustaining impact of the flowing water, the rotation of the wheel is continued, leading to the blades contacting, and separating from the water one by one. For the EMG, when the rotator of EMG is rotating, every copper coil will cut magnetic induction line continually and the total magnetic flux in each coil will keep changing over time. According to the Faraday's law, the open-circuit voltage can be generated in every coil. Owing to the four coils are connected with the external load, constituting a closed loop, the current signals can be observed. As a result, as long as the rotator keeps rotating, the W-TENG, the D-TENG, and the EMG can continuously produce electric power.

For measuring the electrical output properties of the hybridized TENG, we used flowing water and wind to be the power source. The curves of the open-circuit voltage (V_{oc}) of the D-TENG and EMG are shown in **Figure 3**a and b, respectively. The V_{oc} values of the D-TENG and EMG are around 500 and 0.8 V, respectively. For the D-TENG, the curves of the short-circuit current (I_{sc}) are illustrated in Figure 3c with the maximum value of 1.8 μA been recorded. For the EMG, the maximum value of I_{sc} is 7 mA and the curves of I_{sc} is depicted in Figure 3d. It is noteworthy that the rotation rate has a significant impact on the electrical output performance of the D-TENG. Hence, we explored the dependence of the open circuit voltage and short circuit current on rotation rate. The results are shown in Figure S1a, clearly indicating that when the rotation rate increases, the corresponding rise in the short circuit current is observed. However, the open circuit voltage has no remarkable variation. For the EMG, although the open circuit voltage is not high, the value of I_{sc} can reach 14 mA. Similarly, we explored the relationship between the output performance and the rotation rate of the EMG. The corresponding curves are illustrated in Figure S1b. It can be seen that a higher rotation speed can contribute to larger value of V_{oc} and I_{sc}. By comparison, EMG can only supply very low voltage which cannot be used for powering electronic devices, however, the voltage from TENG can be always maintained at a high level, which is independent of frequency. This feature of TENG will be advantageous for harvesting low-frequency mechanical energy, which can fill in gaps at low rotation speed. For the W-TENG, as illustrated in Figure 1a, it has a treble-layer structure. The bottomed layer is Al electrode with nanopores, which will further increase the effective contact area and enhance the electrical output of

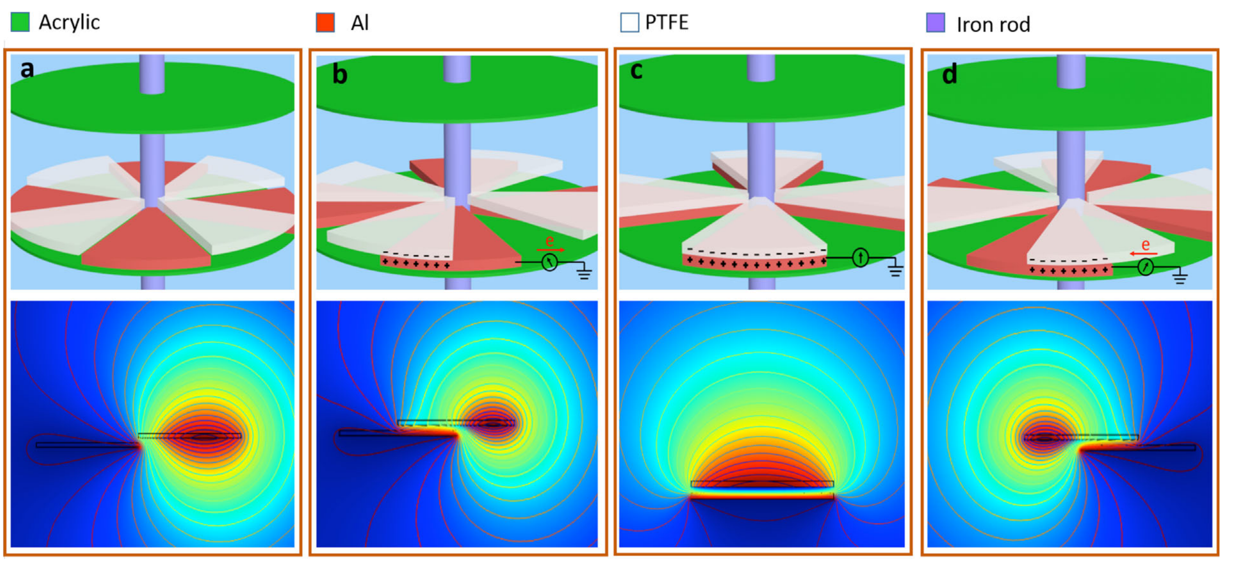

Figure 2. Schematic diagrams of the working principle of the D-TENG. The diagrams illustrate the cross-sectional schematic of charge distribution and potential distribution simulated by COMSOL in four states of D-TENG a–d).

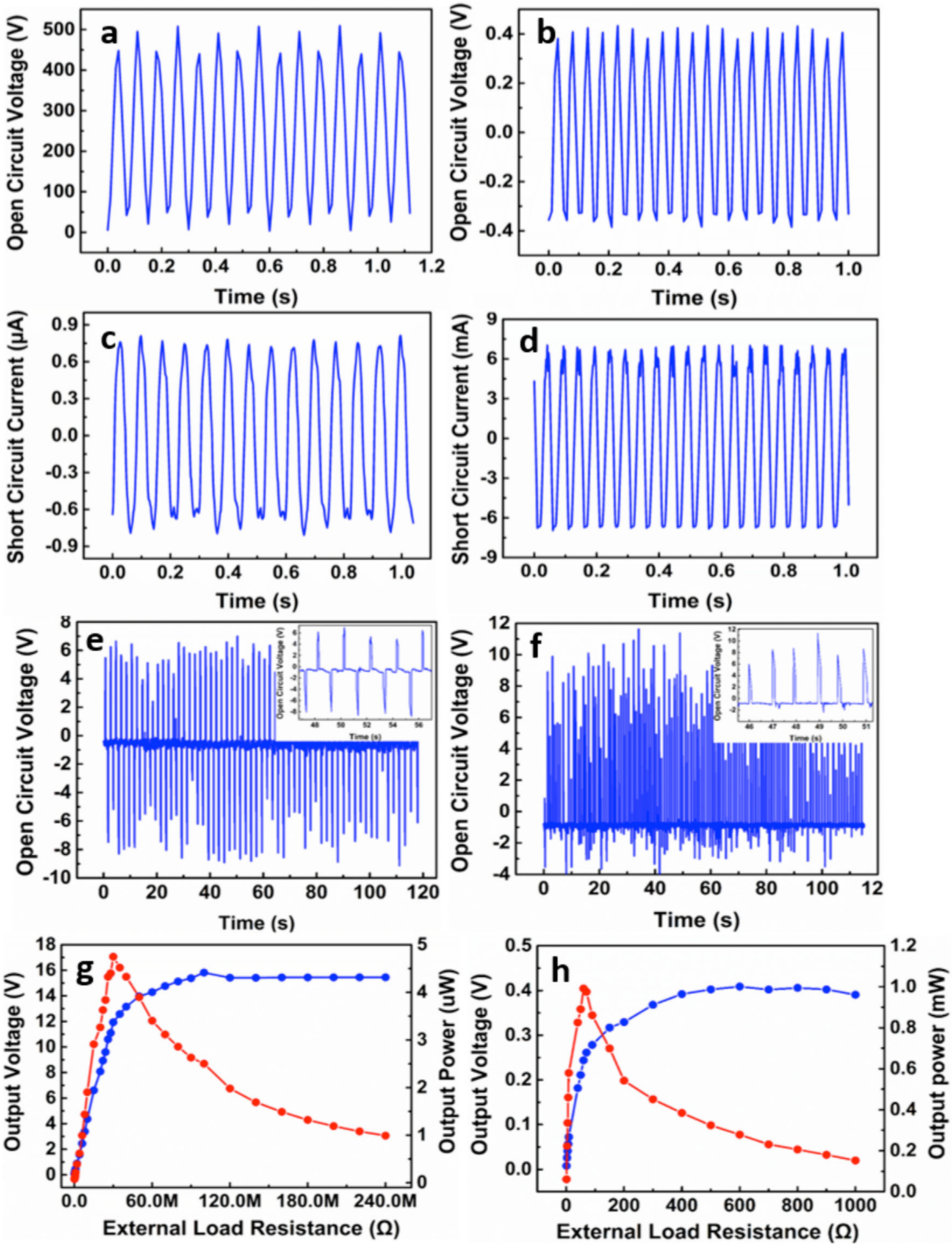

Figure 3. The V_{oc} curves of the D-TENG a), the EMG c), and the W-TENG e). The I_{sc} curves of the D-TENG b), the EMG d), and the W-TENG f). The dependence of the output voltage and power on the external load resistance of the TENG g) and EMG h) before using the transformer.

W-TENG. The middle layer is forward-polarized PVDF thin film and the top layer is PTFE film. To show the effect of the polarized PVDF, we also performed the contrast experiment by using a W-TENG with nonpolarized PVDF film and the curves of V_{oc} and I_{sc} are illustrated in Figure 3e and f, respectively. The corresponding magnified views are plotted in the insets. From the Figure 3e, it can be seen that the W-TENG with nonpolarized PVDF film can produce alternating voltages and the peak value can get 8 V. However, when the forward-polarized PVDF film was attached with the W-TENG, the positive output voltage increases to 12 V with the negligible negative voltage, confirming that the forward-polarized PVDF can enhance the output performance of TENGs. This occurs due to the influence of intrinsic dipole moments on the characteristic potential energy on the surface of PVDF thin films.[31]

As a power source, working under the matched resistance can maximize the out power. However, as we all know, the characteristics of TENG and EMG are quite different. Under the certain rotation rate, the TENG has the large internal resistance and it can be equivalent to a voltage source. However, the EMG can be regarded as a current source with a smaller internal resistance.[32,33] The curves of the output voltage and power on the external load resistance of the TENG and EMG are illustrated in Figure 3g and h, respectively. Specifically, the TENG was measured at various load resistances ranging from 100 KΩ to 240 MΩ, and the instantaneous maximum power of 4.75 μW appears at load resistance of 30 MΩ, as illustrated in Figure 3g. The EMG can achieve the maximal power of 9.91 mW at the load resister of 60 Ω. These results reveals that the TENG and the EMG cannot deliver the maximal output power simultaneously under the same external load due to the huge difference of internal resistances.[34,35]

On the one hand, to solve the mentioned-above problem, we need to use transformers to adjust the output resistances of EMG and TENG. On the other hand, the alternating current (AC) is not suitable for charging batteries or capacitors. Moreover, the AC pulses may not directly satisfy the need of some small electronics, because of the requirement for a constant DC current or the higher power consumption. As a result, it is necessary to use rectifier bridges and transformers to convert AC signals into usable power sources. **Figure 4**a displays a charging curve of a lithium ion battery (10 mAh) with the operating circuit diagram presented in the inset.[36,37] In 270 s, the battery was charged to 3 V by the hybrid NG. When a capacitor is charged by the hybrid NG, it took about 3 s to charge the capacitor to 2 V, as is illustrated in Figure 4b. Compared with that using EMG and D-TENG individually or simultaneously, the hybrid device shows the shortest time to charge the capacitor. The result reveals that, by hybridizing the NGs, the hybrid device can be more effectively store electricity in energy cells. To verify the hybrid NG can be used as a direct power source, Figure 4c shows a letter sign "W" consisted of several LEDs is lit by our device when the wind blows it. The corresponding circuit diagram is plotted in the inset. Flowing water is also a source of flow kinetic energy. As is illuminated in Figure 4d, when water is flowing over our device, the PH sensor can be driven, indicating a self-powered PH tester system can be constructed based on the hybrid NG.[38–41]

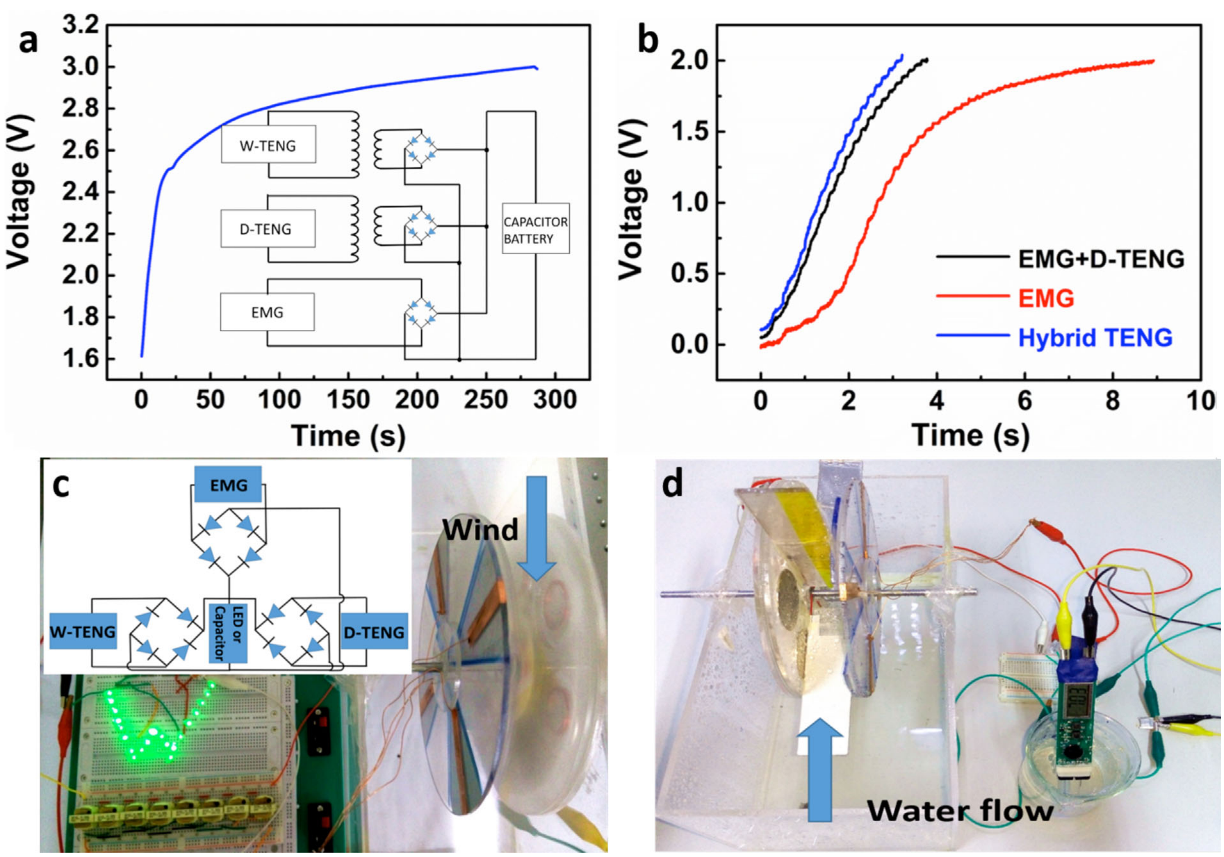

Figure 4. The lithium-ion battery (10 mAh) charging curves of hybrid TENG a). The capacitor (470 μF) charging curves of EMG + TENG, EMG, and Hybrid TENG b). The photography of LED bulbs driven by the hybrid TENG c) and inset shows the diagram of the rectifying circuit. The self-powered PH tester system based on the hybrid TENG d).

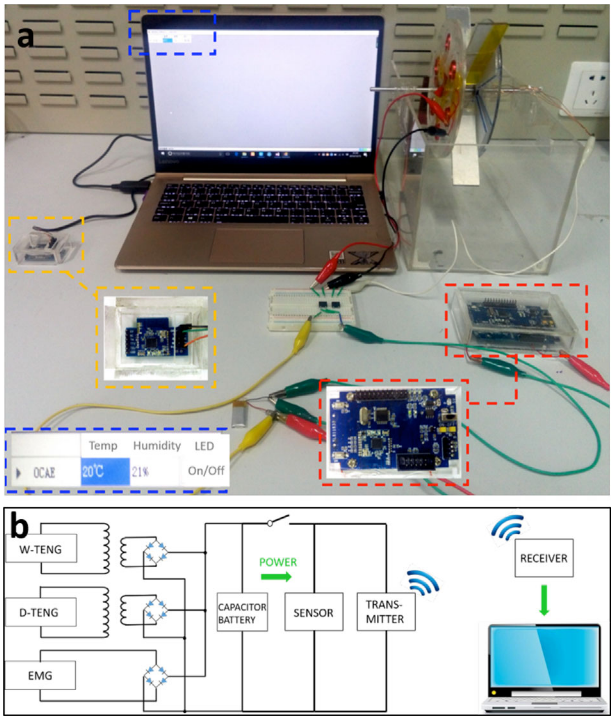

Figure 5. Demonstration of the self-powered, wireless temperature, and humidity sensor systems a). The schematic diagram of the self-powered, wireless temperature, and humidity sensor systems b).

To further exploit the applications of the hybrid NG, **Figure 5**a exhibits the real photograph. The schematic diagram of the constructed self-powered wireless temperature and humidity sensing system is plotted in Figure 5b, which is composed of a hybrid NG, a simple power management system, a sensing system, and a wireless signal transceiver module. The receiver is connected with a laptop, while the transmitter is powered by the hybrid NG. The hybrid NG can drive the temperature and humidity sensor, when the hybrid NG is being actuated by flowing water and wind. More details are presented in Movie 1 and 2. The temperature and humidity values can be displayed in real time on the laptop screen, which is also can be seen in Movie 2.

3. Conclusions

In summary, the hybrid NG consisted of a W-TENG, a D-TENG, and an EMG has been developed for simultaneously harvesting mechanical energies from flowing water and wind. The hybrid NG exhibited the excellent output performance and can be used as a direct power source. In addition, the hybrid energy device can be employed to fabricate different self-powered systems. It is demonstrated that a self-powered wireless temperature and humidity sensor system can be constructed based on the hybrid NG. Our work provides a novel approach to grabbing multiple energies from the environment based on hybrid NGs, which can be widely adopted in environmental ecological monitoring.

Supporting Information

Supporting Information is available online from Wiley Online Library or from the author.

Acknowledgements

This work is sponsored by the National Key Research and Development Program of China (No. 2016YFB0700305-05), the National Natural Science Foundation of China (No. 61504019), the Scientific and Technological Projects for Distinguished Young Scholars of Sichuan Province (No. 2017JQ0016), China Postdoctoral Science Foundation (No. 2017T100687 and 2015M580783), Postdoctoral Research Project of Sichuan Province (No. 20160514), and the Fundamental Research Funds for the Central Universities of China (No. ZYGX2016J046).

Conflict of Interest

The authors declare no conflict of interest.

Keywords

Hybrid nanogenerator, Mechanical energy, Self-powered, Triboelectric nanogenerator

Received: October 5, 2017
Revised: October 30, 2017
Published online: November 23, 2017

[1] F. R. Fan, Z. Q. Tian, Z. L. Wang, *Nano Energy* **2012**, *2*, 328.
[2] Y. Hu, Z. L. Wang, *Nano Energy* **2015**, *14*, 3.
[3] Z. L. Wang, *ACS Nano* **2013**, *7*, 9533.
[4] Z. L. Wang, *Faraday Discuss.* **2014**, *176*, 447.
[5] Z. L. Wang, G. Zhu, Y. Yang, S. H. Wang, C. F. Pan, *Mater. Today* **2012**, *15*, 532.
[6] Z. L. Wang, W. Z. Wu, *Angew. Chem. Int. Ed.* **2012**, *51*, 11700.
[7] S. P. Beeby, M. J. Tudor, N. M. White, *Meas. Sci. Technol.* **2006**, *17*, 175.
[8] H. L. Zhang, S. J. Zhang, G. Yao, Z. L. Huang, Y. H. Xie, Y. J. Su, W. Q. Yang, C. H. Zheng, Y. Lin, *ACS Appl. Mater. Interfaces* **2015**, *51*, 28142.
[9] J. Chen, G. Zhu, W. Yang, Q. Jing, P. Bai, Y. Yang, T. C. Hou, Z. L. Wang, *Adv. Mater.* **2013**, *25*, 6094.
[10] G. Liu, Q. Leng, J. Lian, H. Guo, Y. Xi, C. Hu, *ACS Appl. Mater. Interfaces* **2015**, *7*, 1275.
[11] J. Bae, J. Lee, S. Kim, J. Ha, B.-S. Lee, Y. Park, C. Choong, J.-B. Kim, Z. L. Wang, H.-Y. Kim, J.-J. Park, U. I. Chung, *Nat. Commun.* **2014**, *5*, 4929.
[12] X. Wang, S. Wang, Y. Yang, Z. L. Wang, *ACS Nano* **2015**, *9*, 4553.
[13] J. Chen, J. Yang, Z. Li, X. Fan, Y. Zi, Q. Jing, H. Guo, Z. Wen, K. C. Pradel, S. Niu, Z. L. Wang, *ACS Nano* **2015**, *9*, 3324.
[14] Y. Yang, H. Zhang, R. Liu, X. Wen, T.-C. Hou, Z. L. Wang, *Adv. Energy Mater.* **2013**, *3*, 1563.
[15] L. Lin, S. Wang, S. Niu, C. Liu, Y. Xie, Z. L. Wang, *ACS Appl. Mater. Interfaces* **2014**, *6*, 3031.
[16] Y. Xie, S. Wang, S. Niu, L. Lin, Q. Jing, Y. Su, Z. Wu, Z. L. Wang, *Nano Energy* **2014**, *6*, 129.
[17] G. S. P. Castle, *J. Electrostat.* **1997**, *40–41*, 13.

[18] L. S. McCarty, G. M. Whitesides, *Angew. Chem. Int. Ed.* **2008**, *47*, 2188.
[19] J. A. Wiles, B. A. Grzybowski, A. Winkleman, G. M. Whitesides, *Anal. Chem.* **2003**, *75*, 4859.
[20] F. R. Fan, L. Lin, G. Zhu, W. Z. Wu, R. Zhang, Z. L. Wang, *Nano Lett.* **2012**, *12*, 3109.
[21] G. Zhu, C. F. Pan, W. X. Guo, C. Y. Chen, Y. S. Zhou, R. M. Yu, Z. L. Wang, *Nano Lett.* **2012**, *12*, 4960.
[22] S. H. Wang, L. Lin, Z. L. Wang, *Nano Lett.* **2012**, *12*, 6339.
[23] X. S. Zhang, M. D. Han, R. X. Wang, F. Y. Zhu, Z. H. Li, W. Wang, H. X. Zhang, *Nano Lett.* **2013**, *13*, 1168.
[24] G. Zhu, Z.-H. Lin, Q. S. Jing, P. Bai, C. F. Pan, Y. Yang, Y. S. Zhou, Z. L. Wang, *Nano Lett.* **2013**, *13*, 847.
[25] Z.-H. Lin, G. Cheng, S. Lee, Z. L. Wang, *Adv. Mater.* **2014**, *26*, 4690.
[26] D. Choi, H. Lee, D. J. Im, I. S. Kang, G. Lim, D. S. Kim, K. H. Kang, *Sci. Rep.* **2013**, *3*, 2037.
[27] J. Chen, Y. Huang, N. Zhang, H. Zou, R. Liu, C. Tao, X. Fan, Z. L. Wang, *Nat. Energy* **2016**, *1*, 16138.
[28] G. Cheng, Z. H. Lin, Z. L. Du, Z. L. Wang, *ACS Nano* **2014**, *8*, 1932.
[29] H. Y. Guo, Z. Wen, Y. L. Zi, M. H. Yeh, J. Wang, L. P. Zhu, C. G. Hu, Z. L. Wang, *Adv. Energy Mater.* **2016**, *6*, 150.
[30] P. Bai, G. Zhu, Y. S. Zhou, S. Wang, J. Ma, G. Zhang, Z. L. Wang, *Nano Res.* **2014**, *7*, 990.
[31] Y. Mao, P. Zhao, G. McConohy, H. Yang, Y. Tong, X. Wang, *Adv. Energy Mater.* **2014**, *4*, 1301624.
[32] Y. Mao, D. Geng, E. Liang, X. Wang, *Nano Energy* **2015**, *15*, 227.
[33] C. Zhang, W. Tang, C. Han, F. Fan, Z. L. Wang, *Adv. Mater.* **2014**, *26*, 3580.
[34] Q. S. Jing, G. Zhu, P. Bai, Y. N. Xie, J. Chen, P. S. Han, Z. L. Wang, *ACS Nano* **2014**, *8*, 3836.
[35] Z. M. Lin, J. Chen, X. S. Li, Z. H. Zhou, K. Y. Meng, W. Wei, J. Yang, Z. L. Wang, *ACS Nano* **2017**, *11*, 8830.
[36] Z. L. Wang, J. Chen, L. Lina, *Energy Environ. Sci.* **2015**, *8*, 2250.
[37] G. Zhu, B. Peng, J. Chen, Q. S. Jing, Z. L. Wang, *Nano Energy* **2015**, *14*, 126.
[38] B. Zhang, J. Chen, L. Jin, W. L. Deng, L. Zhang, H. Zhang, M. Zhu, W. Yang, Z. L. Wang, *ACS Nano* **2016**, *10*, 6241.
[39] Y. Zi, L. Lin, J. Wang, S. H. Wang, J. Chen, X. Fan, P. K. Yang, F. Yi, Z. L. Wang, *Adv. Mater.* **2015**, *27*, 2340.
[40] G. Zhu, J. Chen, T. Zhang, Q. Jing, Z. L. Wang, *Nat. Commun.* **2014**, *5*, 3426.
[41] J. Wang, H. Zhang, Y. Xie, Z. Yan, Y. Yuan, L. Huang, Y. Lin, *Nano Energy* **2017**, *33*, 418.